ENCIT 2018

ABCM Associação Brasileira de Engenharia e Ciências Mecânicas

17th Brazilian Congress of Thermal Sciences and Engineering
November 25th-28th, 2018, Águas de Lindóia, SP, Brazil

ENCIT2018-0035
EFFECT OF THE FLOW MACRO-SCALE ON THE EFFECTIVE STRESSES IN DENSE GAS-SOLID FLUIDIZED FLOWS

Joseph MOUALLEM
Seyed Reza Amini NIAKI
Christian C. MILIOLI
Fernando E. MILIOLI
Department of Mechanical Engineering, School of Engineering of Sao Carlos, University of Sao Paulo, 13566-590 Sao Carlos-SP, Brazil
josephmouallem@usp.br, r.amini@usp.br, ccosta@sc.usp.br, milioli@sc.usp.br

Abstract. *Results of highly resolved simulations, filtered in space and time, are used to generate sub-grid closure models for large scale simulations of gas-solid fluidized flows. Actual closures provide a good qualitative description of gas-solid flows but their quantitative accuracy remains an issue. Enhancements over the sub-grid filtered parameters are required. Among these parameters are the effective stresses. Recent studies showed that macro-scale parameters such as gas flow Reynolds number and domain average solid volume fraction present a considerable effect over the filtered parameters in dilute gas solid flows. Thus, macro-scale parameters should be accounted for in sub-grid closure models. This study extends the previous findings and analysis (Mouallem et al., "Effect of the flow macro-scale on the effective stresses in gas-solid riser flows", COBEM2017). It has been shown that the effect of macro-scale parameters diminishes when shifting from dilute to dense flows.*

Keywords: *Gas-particle flow, Fluidization, Two-fluid model, Sub-grid modeling, Effective stresses*

1. INTRODUCTION

Modeling in gas-particle flows has always been a challenge for researchers. Two-fluid modeling represents one important line of research in this area. It is widely used in large scale simulations of such flows (e.g. Gidaspow, 1994). This method successfully describes the qualitative properties of such flows, but fails when one is looking to carry out an accurate quantitative analysis . This failure stems from the incapability of actual closure models to accurately describe relevant sub-grid effects. Closures for effective stresses represent one of the problems to tackle. This article is intended to be a contribution in that context by discussing possible sub-grid modeling enhancement for effective stresses. Closures for effective stresses, which are usually expressed as effective pressures and dynamic viscosities, have been derived empirically as well as theoretically (Gidaspow and Ettehadieh, 1983; Bouillard et al., 1989; Tsuo and Gidaspow, 1990; Sinclair and Jackson, 1989; Campbell and Wang, 1991; Massoudi et al., 1992; Gidaspow, 1994; Enwald et al., 1996; Sinclair, 1997). An usual procedure for deriving sub-grid effective closures consists on averaging or filtering over results of highly resolved simulations with microscopic two-fluid modeling. In those formulations, both phases are assumed to behave as a newtonian fluid. For the solid phase, pressure, dynamic viscosity and bulk viscosity are all brought from the kinetic theory of granular flows (Jenkins and Savage, 1983; Lun et al., 1984; Garzó and Dufty, 1999; Gidaspow, 1994). This theory is analogous to the kinetic theory of dense gases. In the latter theory, fluid properties (pressure, viscosity) are determined based on the thermodynamic temperature, while in the first theory, a granular temperature is defined which allows us to determine the solid pressure and viscosity. A number of works have been developed which provided effective stresses analyses and correlation departing from results of highly resolved simulations with microscopic two-fluid modeling (Agrawal et al., 2001; Andrews IV et al., 2005; Igci et al., 2008; Milioli and Milioli, 2011; Igci and Sundaresan, 2011a,b; Parmentier et al., 2012; Ozel et al., 2013; Milioli et al., 2013; Agrawal et al., 2013; Schneiderbauer and Pirker, 2014; Sarkar et al., 2016). In general, the highly resolved simulations provide meso-scale solutions over which filtering is performed to provide sub-grid filtered data for parameters such as the effective pressures and viscosities of both phases. At the current state of affairs, those effective parameters are correlated to inside filter averaged parameters only, disregarding any effects of the outside flow topology.

In a recent work (Mouallem et al., 2017), the effect of two macro-scale variables, the average solid volume fraction and average gas Reynolds number, over the filtered parameters has been investigated for riser gas-solid flows. It has been found that these macro-scale variables affect considerably the flow topology and filtered parameters. Moreover, these macro-scale variables should be accounted for in sub-grid closure models in a step forward to improve their accuracy. In this previous work, however, only dilute gas-solid flow conditions were considered.. To get a better understanding of the

effect of macro-scale variables over the whole range of gas solid flows, this work extended the previous study to the dense regime.

2. METHOD

Highly Resolved Simulations (HRS) are performed using a microscopic two-fluid model, as described in Agrawal et al. (2001). The filtered two-fluid model is used for Large Scale Simulations (LSS). By averaging results from the HRS, one can derive the required sub-grid closures needed for the undetermined terms in the filtered two-fluid model. This is illustraded in "Figure 1". There is a considerable literature describing two-fluid modeling applied to gas-particle fluidized flows (Anderson and Jackson, 1967; Gidaspow, 1994; Enwald et al., 1996). Both the microscopic and filtered formulations of the two-fluid model are described next, in order to show where the sub-grid closures are needed, and the referred means by which they are derived.

2.1 Microscopic Two-Fluid model

The microscopic formulation of the two-fluid model as applied to gas-particle fluidized flows is partially presented in "Tab. 1", emphasizing the formulation of main concern in the present work. Micro-scale closures for the solid phase stresses are established by applying the kinetic theory of granular flows (KTGF) (Jenkins and Savage, 1983; Lun et al., 1984; Gidaspow, 1994; Garzo et al., 1999), where the continuous solid phase micro-scale properties are derived as a function of a granular temperature determined from a pseudo-thermal energy balance. These closures are the same as the ones assumed by Agrawal et al., 2001. In addition to the conservative equations of continuity and momentum, the microscopic model also requires a conservation equation of granular energy to be resolved as well (Gidaspow, 1994; Agrawal, 2001). "Equations (2.1), (22), (23), and (24)" represent the continuity and momentum conservation equations for the gas and solid phases. "Equation (25)" represents the volumetric continuity. "Equation (26)" represents the conservation of granular energy. Closures for the stresses are presented next in the table. Other closures (for the granular energy conservation, and interface forces) can be found in (Agrawal et al., 2001).

Table 1: Two-fluid model

Continuity and momentum conservation equations :

$$\frac{\partial}{\partial t}\left(\rho_g \phi_g\right) + \nabla \cdot \left(\rho_g \phi_g \mathbf{v}_g\right) = 0 \tag{2.1}$$

$$\frac{\partial}{\partial t}\left(\rho_s \phi_s\right) + \nabla \cdot \left(\rho_s \phi_s \mathbf{v}_s\right) = 0 \tag{2.2}$$

$$\frac{\partial}{\partial t}\left(\rho_g \phi_g \mathbf{v}_g\right) + \nabla \cdot \left(\rho_g \phi_g \mathbf{v}_g \mathbf{v}_g\right) = -\phi_g \nabla \cdot \boldsymbol{\sigma}_g - \mathbf{M}_I + \rho_g \phi_g \mathbf{g} \tag{2.3}$$

$$\frac{\partial}{\partial t}\left(\rho_s \phi_s \mathbf{v}_s\right) + \nabla \cdot \left(\rho_s \phi_s \mathbf{v}_s \mathbf{v}_s\right) = -\nabla \cdot \boldsymbol{\sigma}_s - \phi_s \nabla \cdot \boldsymbol{\sigma}_g + \mathbf{M}_I + \rho_s \phi_s \mathbf{g} \tag{2.4}$$

Volumetric continuity :

$$\phi_g + \phi_s = 1 \tag{2.5}$$

Granular energy conservation equation :

$$\frac{3}{2}\left[\frac{\partial}{\partial t}\left(\rho_s \phi_s \Theta\right) + \nabla \cdot \left(\rho_s \phi_s \mathbf{v}_s \Theta\right)\right] = -\boldsymbol{\sigma}_s{:}\nabla \mathbf{v}_s + \nabla \cdot \left(\kappa_s \nabla \Theta\right) + \Gamma_{slip} - J_{coll} - J_{vis} \tag{2.6}$$

Closure for stresses :

$$\boldsymbol{\sigma}_l = \left[P_l - \left(\lambda_l + \frac{2}{3}\mu_l\right)\left(\nabla \cdot \mathbf{v}_l\right)\right]\mathbf{I} - 2\mu_s \boldsymbol{s}_l \qquad l = g, s \tag{2.7}$$

$$\boldsymbol{s}_l = \frac{1}{2}\left[\nabla \mathbf{v}_l + \left(\nabla \mathbf{v}_l\right]^T\right) - \frac{1}{3}\left(\nabla \cdot \mathbf{v}_l\right)\mathbf{I} \qquad l = g, s \tag{2.8}$$

$$\mu_g = constant \qquad \lambda_g = 0 \tag{2.9}$$

$$\mu_s = \frac{(2+\alpha)}{3}\left\{\frac{\xi^*}{g_0 \eta (2-\eta)}\left(1 + \frac{8}{5}\phi_s \eta g_0\right)\left(1 + \frac{8}{5}\eta(3\eta - 2)\phi_s g_0\right) + \frac{6}{5}\eta \mu_b\right\} \tag{2.10}$$

$$\lambda_s = \eta \mu_b - \frac{2}{3}\mu_s \qquad \alpha = 1.6 \tag{2.11}$$

$$\mu_b = \frac{256 \xi \phi_s^2 g_0}{5\pi} \qquad \xi^* = \frac{\xi}{1 + \frac{2\beta\xi}{(\rho_s \phi_s)^2 g_0 \Theta}} \qquad \xi = \frac{5\rho_s d_p (\pi\Theta)^{\frac{1}{2}}}{96} \tag{2.12}$$

$$P_s = \rho_s \phi_s (1 + 4\eta \phi_s g_0)\Theta \tag{2.13}$$

$$g_0 = \frac{1}{1 - \left(\frac{\phi_s}{\phi_{s,max}}\right)^{\frac{1}{3}}} \qquad \phi_{s,max} = 0.65 \qquad \eta = \frac{1+e}{2} \tag{2.14}$$

Other required closures can be found in (Agrawal et al., 2001)

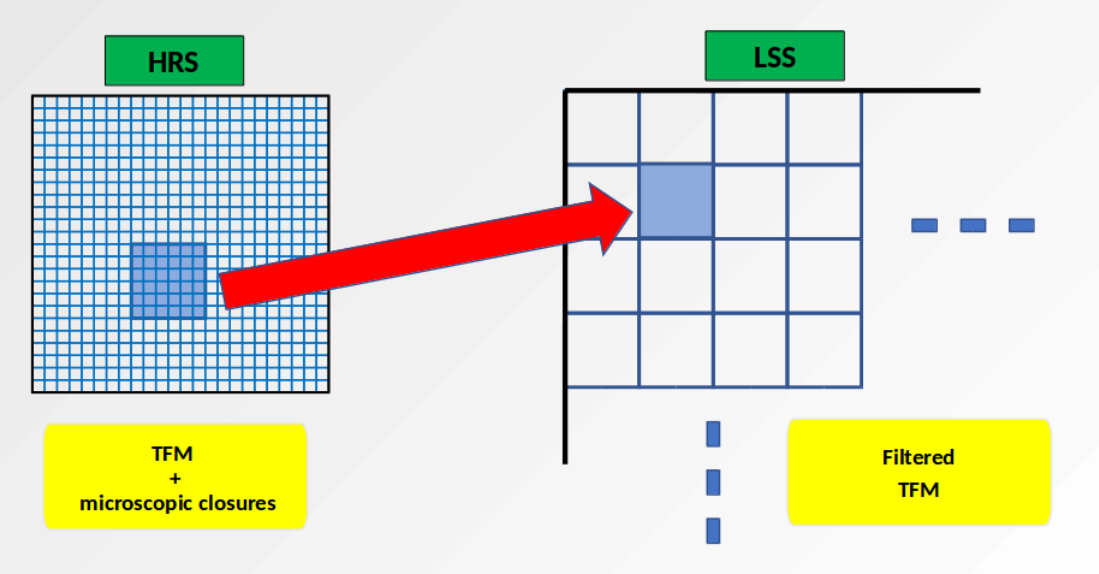

Figure 1: Two-Fluid models for Highly Resolved Simulations (HRS) and Large Scale Simulations (LSS)

2.2 Filtered Two-Fluid model

The two-fluid model with microscopic closures can be transformed into coarse-grained (or filtered) equations through filtering, using spatial averaging over a certain length scale (filter size). This procedure provides a filtered two-fluid model presented in "Tab. 2".

As a results of the averaging process, filtered parameters appear which require constitutive formulations to close the set of equations. Regarding the effective stresses of main interest in the present work, the terms that require closure are the particle and gas effective pressures and viscosities, represented by "Eq (222) and (223)" respectively. Just as done for the microscopic model given in "Tab. 1", the filtered model in "Tab. 2" is only presented partially, emphasizing the formulation of main concern in the present work. Further closures for the filtered model can be found in (Agrawal et al., 2001)

Table 2: Filtered two-fluid model

Filtered continuity and momentum conservation equations:

$$\frac{\partial}{\partial t}\left(\rho_g \overline{\phi}_g\right) + \nabla \cdot \left(\rho_g \overline{\phi}_g \widetilde{\mathbf{v}}_g\right) = 0 \tag{215}$$

$$\frac{\partial}{\partial t}\left(\rho_s \overline{\phi}_s\right) + \nabla \cdot \left(\rho_s \overline{\phi}_s \widetilde{\mathbf{v}}_s\right) = 0 \tag{216}$$

$$\frac{\partial}{\partial t}\left(\rho_g \overline{\phi}_g \widetilde{\mathbf{v}}_g\right) + \nabla \cdot \left(\rho_g \overline{\phi}_g \widetilde{\mathbf{v}}_g \widetilde{\mathbf{v}}_g\right) = -\overline{\phi}_g \nabla \widetilde{\boldsymbol{\sigma}}_g - \nabla \cdot \boldsymbol{\tau}'_g - \left(\mathbf{B}'_{gs} + \overline{\mathbf{M}}_I\right) + \rho_g \overline{\phi}_g \mathbf{g} \tag{217}$$

$$\frac{\partial}{\partial t}\left(\rho_s \overline{\phi}_s \widetilde{\mathbf{v}}_s\right) + \nabla \cdot \left(\rho_s \overline{\phi}_s \widetilde{\mathbf{v}}_s \widetilde{\mathbf{v}}_s\right) = -\nabla \cdot \overline{\boldsymbol{\sigma}}_s - \nabla \cdot \boldsymbol{\tau}'_s - \overline{\phi}_s \nabla \cdot \widetilde{\boldsymbol{\sigma}}_g + \left(\mathbf{B}'_{gs} + \overline{\mathbf{M}}_I\right) + \rho_s \overline{\phi}_s \mathbf{g} \tag{218}$$

Filtered volumetric continuity:

$$\overline{\phi}_g + \overline{\phi}_s = 1 \tag{219}$$

Closure for effective stresses :

$$\boldsymbol{\tau}'_\ell = \rho_\ell \overline{\phi}_\ell (\mathbf{v}_\ell \mathbf{v}_\ell) + \rho_\ell \overline{\phi}_\ell \widetilde{\mathbf{v}}_\ell \widetilde{\mathbf{v}}_\ell = P_{eff,\ell} \mathbf{I} - 2\mu_{eff,\ell} \widetilde{\mathbf{s}}_\ell \qquad \text{for} \qquad \ell = g, s \tag{220}$$

$$\widetilde{\mathbf{s}}_\ell = \frac{1}{2}\left(\nabla \widetilde{\mathbf{v}}_\ell + \left(\nabla \widetilde{\mathbf{v}}_\ell\right)^T\right) - \frac{1}{3}\left(\nabla \cdot \widetilde{\mathbf{v}}_\ell\right)\mathbf{I} \qquad \text{for} \qquad \ell = g, s \tag{221}$$

$$P_{eff,\ell} = \frac{1}{3} tr(\boldsymbol{\tau}'_\ell) \qquad \text{for} \quad \ell = g, s \tag{222}$$

$$\mu_{eff,\ell} = \frac{|\boldsymbol{\tau}'_{shear,\ell}|}{2|\widetilde{\mathbf{s}}_{shear,\ell}|} \tag{223}$$

Other required closures can be found in (Agrawal et al.,2001)

2.3 Numerical Simulations

Following (Mouallem et al., 2017), numerical simulations were performed using the open source Fortran code MFIX (Syamlal et al.,1993; Syamlal et al.,1998). Periodic boundaries, in all directions, were applied for a 16 cm x 16 cm domain size. According to literature (Agrawal et al., 2001), a grid size between 1 and 2 mm provides grid size independent results.

Following this, a numerical mesh of 128x128 was used, resulting in a grid size of 1.25 mm.

The domain average gas Reynolds number, fixed in each simulation, is given by:

$$\langle Re_g \rangle = \frac{d_p \rho_g \langle \phi_g \rangle \langle v_{g,y} \rangle}{\mu_g} \tag{224}$$

Where $\langle v_{g,y} \rangle$ represents the domain averaged gas phase velocity in the axial (vertical) direction. The domain average solid volume fraction $\langle \phi_s \rangle$ was also set constant in the various simulations, at the values of 0.35, 0.45 and 0.50. For each domain averaged solid volume fraction, the domain average gas Reynolds number was calculated for the suspension case. A suspension simulation consists of applying a pressure gradient in the vertical direction to exactly balance the weight of the gas and solid mixture existing in the domain:

$$\frac{\Delta P_y}{L} = \rho_s \langle \phi_s \rangle g + \rho_g \langle \phi_g \rangle g \tag{225}$$

After calculating the suspension case domain average gas Reynolds number $\langle Re_g \rangle_{susp}$, the actual $\langle Re_g \rangle$ is set fixed in each simulation by composing a ratio ${}^{\langle Re_g \rangle}/_{\langle Re_g \rangle_{susp}}$ = 1.00, 8.15, 16.30 and 24.45 for each $\langle \phi_s \rangle$ considered.

Gas and solid properties were set as follows: the particle diameter $d_p = 7.5\text{x}10^{-5}m$, the particle density $\rho_s = 1.3kg/m^3$, the gas density $\rho_g = 1.3kg/m^3$, the gas viscosity $\mu_g = 1.8\text{x}10^{-5}kg/m.s$, the coefficient of restitution $e_p = 0.9$. From those properties, the terminal settling velocity of a particle$v_t = 0.2184m/s$, and the particle Froude number $Fr = v_t^2/(gd_p) = 64.85$.

2.4 Two-bin filtering

"Figure 2" represents a snapshot of the simulation in the statitical steady state regime. The blue color represents the gas phase, while the red color represents the solid phase. The red square represents the filter size. The filter size denotes the area where the averaging proccess will be conducted. This area is yellow highlighted. Once the flow field enters the statistical steady state regime, the averaging proccess begins. A huge number of simulation snapshots was taken in order to ensure reliable statistics. Once all the parameters inside the filter size are averaged, the values are classified by ranges of filtered solid volume fraction and filtered slip velocity (named markers). The filter is then displaced all over the domain and the filtered parameters are further averaged into appropriate bins for the various ranges of the markers. Once we get all the information from a specific snapshot, the same procedure is conducted for the next snapshot. Note that averaging in space and averaging in time give statistically equivalent results.

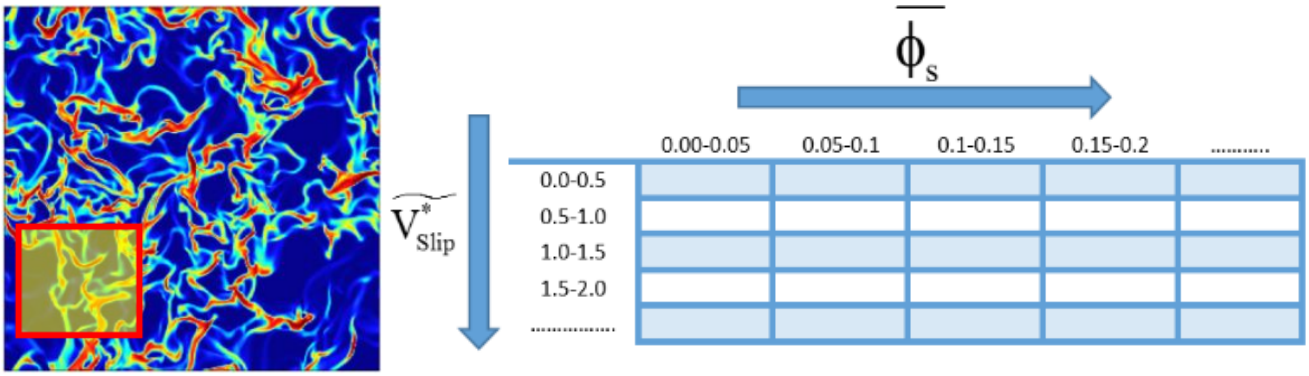

Figure 2: Illustration of a snapshot of solid volume fraction and a two-binning table.

3. Results and discussion

The results presented here are only for a unique dimensionless filtered slip velocity $\tilde{\text{v}}_{\text{slip,y}}/\text{v}_\text{t} = 0.21$, and the dimensionless filter size $\Delta_\text{f}/(\text{v}_\text{t}^2/\text{g}) = 4.112$. The effective pressures and viscosities of concern are made dimensionless by the amount $\rho_s v_t^2$ and $\rho_s v_t^3/g$, respectively. 64 columns and 80 rows formed the two-bin table. The average solid volume fraction $\overline{\phi_s}$ varied from $\overline{\phi_s}_{min} = 0.005$ up to $\overline{\phi_s}_{max} = 0.645$, while the average slip velocity varied from $\overline{V_{slip}}_{min} = 0.001$ cm/s up to $\overline{V_{slip}}_{max} = 111.6$ cm/s. These values were found suitable to catch all the flow properties.

"Figures 3a, 3b, and 3c" show the variation of the effective solid and gas pressures, $P_{eff,s}$ and $P_{eff,g}$, for domain average solid volume fractions $\langle \phi_s \rangle = 0.35, 0.45$ and 0.50, respectively, as a function of the filtered solid volume fraction $\overline{\phi}_s$, for Reynolds number ratios varying from 1.00 to 24.45. As seen, the domain average gas Reynolds number has a significant effect over the effective pressures for both phases. A noticeable variation can be seen for $\langle \phi_s \rangle = 0.35$ especially for $0.3 < \overline{\phi_s} < 0.4$. Variations of up to one order of magnitude can be observed.

"Figure 3d" presents the effective pressure P_{eff} of both phases for $\langle \phi_s \rangle = 0.35$ and 0.45, and Reynolds number

ratios 1 and 24.45. For both phases, small differences can be seen between the profiles for $\langle\phi_s\rangle = 0.35$ and 0.45 at low Reynolds number ratios. The difference decreases for the higher Reynolds ratio 24.45. Very remarkable difference among the profiles can be observed for the high Reynolds ratio 24.45, when the results for $\langle\phi_s\rangle = 0.35$ and 0.45 (symbols) are compared to those for Reynolds Ratio = 1(lines) . One possible explanation for this behavior can be related to the increased degree of homogeneity of a dilute flow at high Reynolds numbers.

"Figures 4a, 4b, and 4c" show the variation of the effective solid and gas viscosities , $\mu_{eff,s}$ and $\mu_{eff,g}$ for the same conditions in 3, that is for domain average solid volume fractions $\langle\phi_s\rangle = 0.35, 0.45$ and 0.50, respectively, as a function of the filtered solid volume fraction $\overline{\phi}_s$, for Reynolds number ratios varying from 1.00 to 24.45. The effective viscosities of both phases are little affected by the domain average gas Reynolds number for all domain average solid volume fractions.

"Figure 4d" presents the effective viscosity μ_{eff} of both phases for the same conditions in "Fig. 3d". In contrast with the behavior seen for P_{eff} in "Fig. 3d", when passing from $\langle\phi_s\rangle = 0.35$ to $\langle\phi_s\rangle = 0.45$, under the low and high Reynolds number ratio of 24.45, the differences among the profiles are relatively small for both phases.

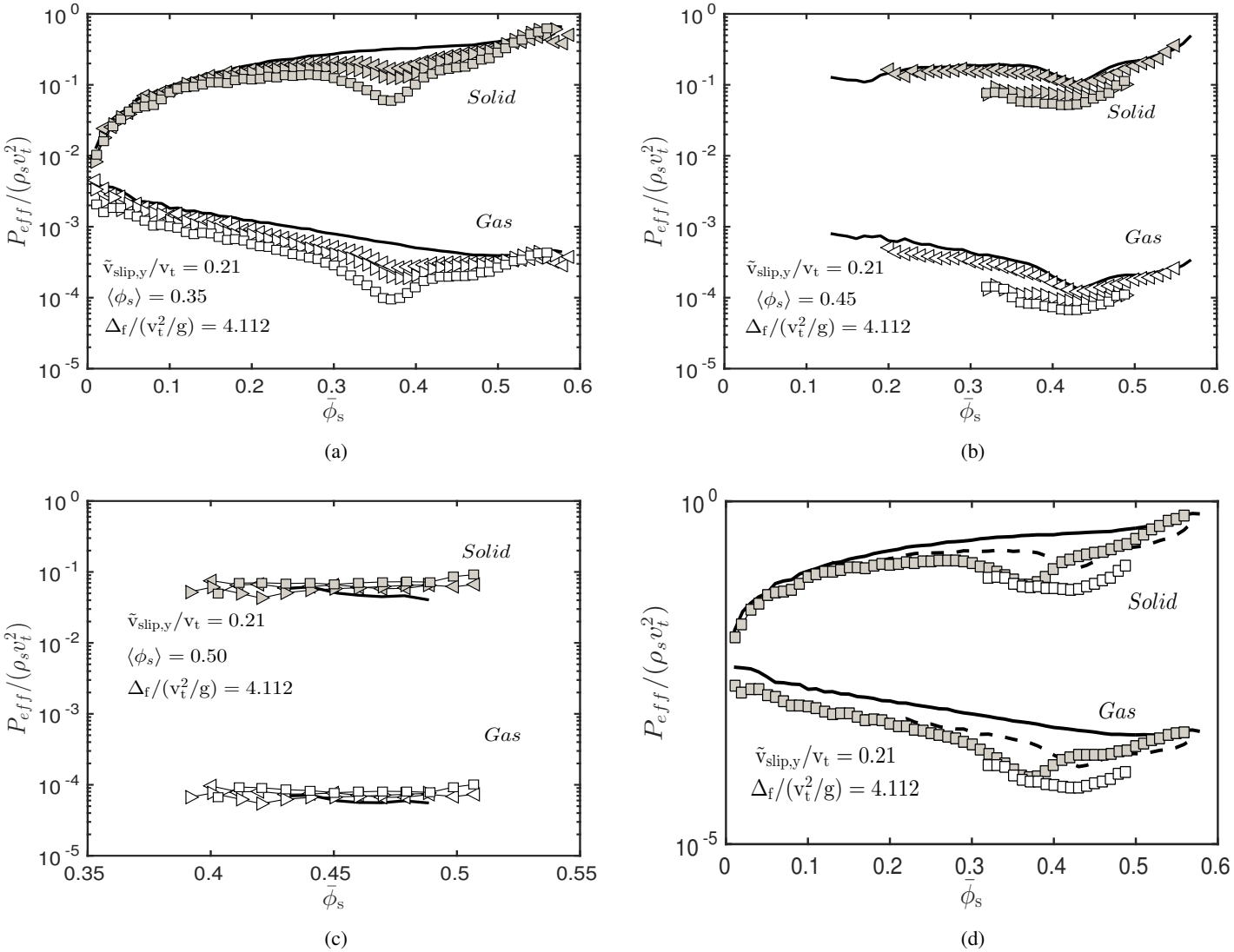

Figure 3: Effective solid and gas pressures, $P_{eff,s}$ and $P_{eff,g}$, as a function of the filtered solid volume fraction, $\overline{\phi}_s$, for various gas Reynolds ratios ${}^{\langle Re_g\rangle}/_{\langle Re_g\rangle_{susp}} = 1(-), 8.15(\triangleleft), 16.30(\triangleright)$, and $24.45(\square)$, for the domain average solid volume fraction $\langle\phi_s\rangle = 0.35$ (a) , 0.45 (b) and 0.50 (c). For figure 3d: the domain average solid volume fractions $\langle\phi_s\rangle$ = 0.35 (continuous line and gray symbols) and 0.45 (dashed line and white symbols), gas Reynolds ratios ${}^{\langle Re_g\rangle}/_{\langle Re_g\rangle_{susp}} =$ 1 (line) and $24.45(\square)$.

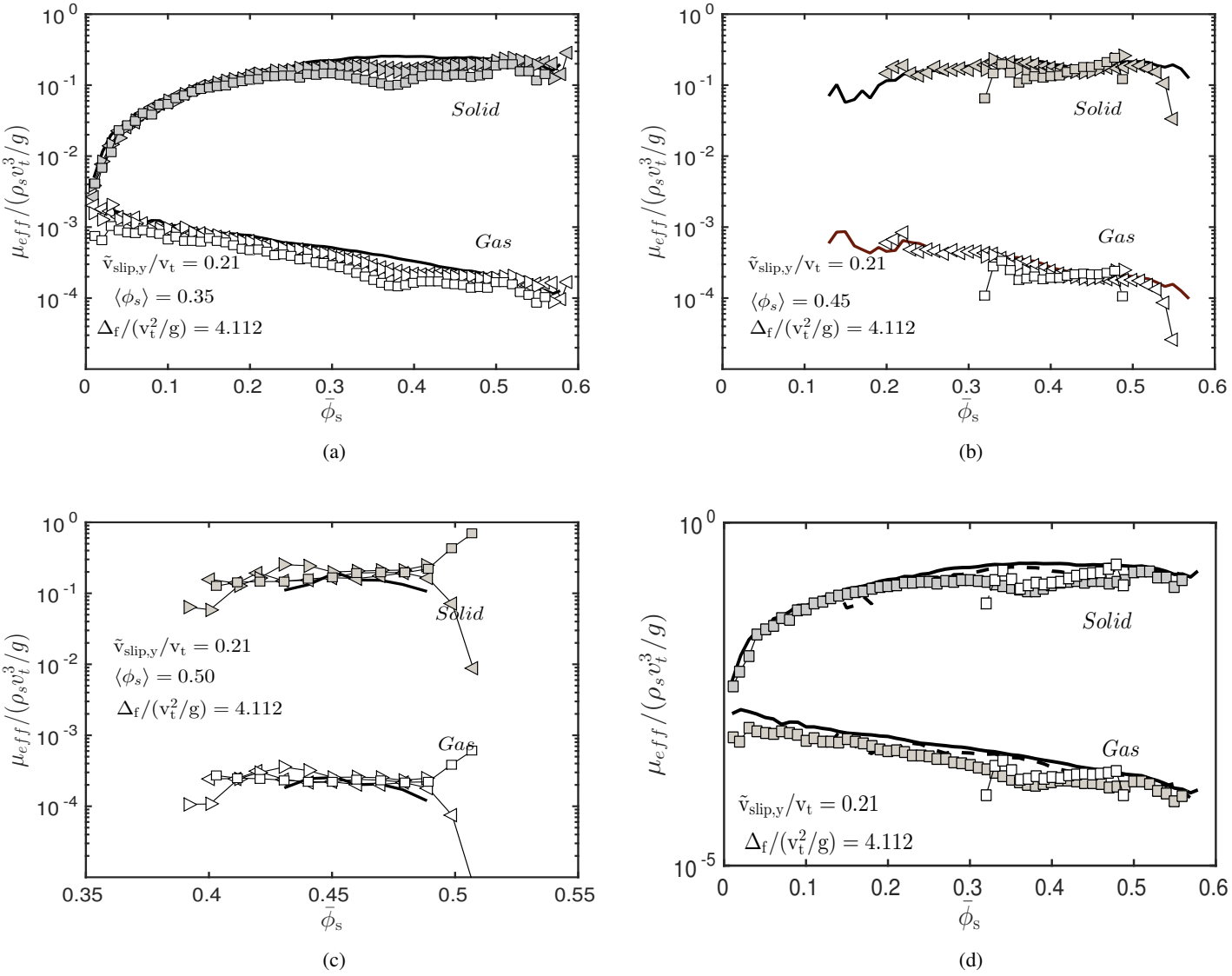

Figure 4: Effective solid and gas dynamic viscosities, $\mu_{eff,s}$ and $\mu_{eff,g}$, as a function of the filtered solid volume fraction, $\overline{\phi}_s$, for various gas Reynolds ratios ${}^{\langle Re_g\rangle}/_{\langle Re_g\rangle_{susp}} = 1(-), 8.15(\triangleleft), 16.30(\triangleright)$, and $24.45(\square)$, for the domain average solid volume fraction $\langle\phi_s\rangle = 0.35$ (a) , 0.45 (b) and 0.50 (c). For figure 4d: the domain average solid volume fractions $\langle\phi_s\rangle$ = 0.35 (continuous line and gray symbols) and 0.45 (dashed line and white symbols), gas Reynolds ratios ${}^{\langle Re_g\rangle}/_{\langle Re_g\rangle_{susp}} = 1$ (line) and $24.45(\square)$.

4. Conclusions

The filtered two-fluid model used in large scale simulations (LSS) presents some unknow terms that need closures. Sub-grid closure models can be obtained through averaging over highly resolved simulation (HRS) data. Effective stresses are among the important parameters requiring closures. To improve the present closure models, the effect of new system variables must be explored. In the current work, the effect of the macro-scale parameters, the domain average solid volume fraction and domain average gas Reynolds number, over the effective stresses was investigated. 2D highly resolved simulations with microscopic two-fluid modeling were performed using the open source code MFIX. Periodic boundaries in all directions were applied over a domain of $16cm$ x $16cm$. Filtering was considered in the statistical steady state flow regime, over a large enough time interval to provide for suitable statistics. Gas Reynolds number were varied from 1.00 to 24.45 times the gas Reynolds number required for the suspension case. For both phases, the effective pressure varied by up to one order of magnitude and the effective viscosity showed very little variation in the concerning range of gas Reynolds number. This is in contrast to what was previously observed under dilute conditions (Mouallem et al., 2017), where the effective pressures varied by up to two orders of magnitude and the effective viscosities varied by up to one order of magnitude, in the same gas Reynolds number range.

5. ACKNOWLEDGEMENTS

This work was supported by The State of São Paulo Research Foundation (FAPESP), The National Council for Scientific and Technological Development (CNPq), and The Coordination for the Improvement of Higher Level Personnel (CAPES), all from Brazil.

6. REFERENCES

Agrawal, K., Loezos, P.N., Syamlal, M. and Sundaresan, S., 2001, *"The role of meso-scale structures in rapid gas-solid flows"* , J. Fluid Mech., Vol. 445, pp. 151-185.

Agrawal, K., Holloway, W., Milioli, C.C., Milioli, F.E. and Sundaresan, S., 2013, *"Filtered models for scalar transport in gas-particle flows"*, Chem. Eng. Science, Vol,. 95, pp. 291-300.

Anderson, T.B. and Jackson, R., 1967, *"Fluid Mechanical Description of Fluidized Beds. Equation of Motion"* ,Indust. Engng. Chem.Fundam., Vol. 6, pp.527-539

Andrews IV, A.T., Loezos, P.N. and Sundaresan, S., 2005, *"Coarse-grid simulation of gas-particle flows in vertical risers"*, Ind. Eng. Chem. Res., Vol. 44, No. 16, pp. 6022-6037.

Bouillard, J.X., Lyczkowski, R.W. and Gidaspow, D., 1989, *"Porosity distributions in a fluidized bed with an immersed obstacle"*, AIChE J., Vol 35, No. 6, pp. 908-922

Campbell, C.S. and Wang, D.G., 1991, *"Particle pressure in gas-fluidized beds"*, J. Fluid Mech., Vol. 227, pp. 495-508.

Enwald, H., Peirano, E. and Almstedt, A.-E., 1996, *"Eulerian Two-Phase Flow Theory Applied to Fluidization"*, Int. J. of Multiphase Flow, Vol. 22, pp.21-66.

Garzó, V. and Dufty, J.W., 1999, *"Dense fluid transport for inelastic hard spheres"*, Phys. Rev. E, Vol. 59, pp. 5895–5911.

Gidaspow, D. and Ettehadieh, B., 1983, *"Fluidization in two-dimensional debs with a jet. Part II. Hydrodynamic modeling"*, Indust. Engng. Chem. Fundam., Vol. 22, pp. 193-201.

Gidaspow, D., 1994, *"Multiphase Flow and Fluidization"*, Academic Press, San Diego, CA, 407p.

Igci, Y., Andrews IV, A.T., Sundaresan, S., Pannala, S. and O'Brien, T., 2008, *"Filtered two-fluid models for fluidized gas-particle suspensions"*, AIChE Journal, Vol. 54, No. 6, pp. 1431-1448.

Igci, Y. and Sundaresan, S., 2011a, *"Constitutive models for filtered two-fluid models of fluidized gas-particle flows"*, Ind. Eng. Chem. Res., Vol. 50, pp. 13190-13201.

Igci, Y. and Sundaresan, S., 2011b, *"Verification of filtered two-fluid models for gas-particle flows in risers"*, AIChE J., Vol. 57, pp. 2691-2707.

Jenkins, J.T. and Savage, S.B., 1983, *"A Theory for the Rapid Flow of Identical, Smooth, Nearly Elastic Spherical Particles"*, J. Fluid. Mech., Vol. 130, pp. 187-202.

Lun, C.K.K., Savage, S.B., Jeffrey, D.J. and Chepurniy, N., 1984, *"Kinetic Theories for Granular Flows: Inelastic Particles in Couette Flow and Singly Inelastic Particles in a General Flow Field"*, J. Fluid. Mech., Vol. 140, pp.223-256

Massoudi, M., Rajagopal, K.R., Ekmann, J.M. and Mathur, M.P., 1992, *"Remarks on the modeling of fluidized systems"*, AIChE J., Vol. 38, No. 3, pp. 471-472.

Mouallem, J., Niaki, S.R.A., Chavez-Cussy, N., Netzlaff, G.J.S., Milioli, C.C. and Milioli, F.E. 2017. *"Effect of the flow macro-scale on effective stresses in gas-solid riser flows"*, In Proceedings of the 24st International Congress of Mechanical Engineering - COBEM2017, Curitiba, Brazil

Milioli, C.C. and Milioli, F.E., 2011, *"On the sub-grid behavior of accelerated riser flows for a high Stokes number particulate"*, Industrial and Engineering Chemistry Research, Vol. 50, pp. 13538-13544.

Milioli, C.C., Milioli, F.E., Holloway, W., Agrawal, K. and Sundaresan, S., 2013, *"Filtered two-fluid models of fluidized gas-particle flows: New constitutive relations"*, AIChE J., Vol. 59, pp. 3265-3275.

Özel, A., Fede, P. and Simonin, O., 2013, *"Development of filtered Euler–Euler two-phase model for circulating fluidised bed: High resolution simulation, formulation and a priori analyses"*, Int. J. Multiphase Flow, Vol. 55 . pp. 43-63.

Parmentier, J-F, Simonin O. and Delsart O., 2012, *"A functional subgrid drift velocity model for filtered drag prediction in dense fluidized bed"*, AIChE J., Vol. 58, pp. 1084-1098.

Sarkar, A., Milioli, F.E., Ozarkar, S., Li, T., Sun, X. and Sundaresan, S., 2016, *"Filtered sub-grid constitutive models for fluidized gas-particle flows constructed from 3-D simulations"*, Chemical Engineering Science, Vol. 152, pp. 443-456.

Schneiderbauer, S. and Pirker, S., 2014, "Filtered and Heterogeneity-Based Subgrid Modifications for Gas–Solid Drag and Solid Stresses in Bubbling Fluidized Beds", AIChE J., Vol. 60, pp. 839-854.

Sinclair, J.L. and Jackson, R., 1989, *"Gas-particle flow in a vertical pipe with particle-particle interactions"*, AIChE Journal, Vol. 35, No. 9, pp. 1473-1486.

Sinclair, J.L., 1997, *"Hydrodinamic Modeling"* , In Circulating Fluidized Beds, ed. J.R. Grace et al., Chapman and Hall. Cap. 5, p.149-180.

Syamlal, M., Rogers, W. and O'Brien, T. J., 1993, *"Theory guide"*, MFIX documentation, Vol. 1, DOE/METEC-94/1004 NTIS/DE9400087, National Technical Information Service, Springfield, VA.

Syamlal, M. 1998, *MFIX Documentation: Numerical Techniques*. DOE/MC-31346-5824. NTIS/DE98002029.

Tsuo, Y.P. and Gidaspow, D., 1990, *"Computation of flow patterns in circulating fluidized beds"*, AIChE J., Vol. 36, No. 6, pp. 885-896.

7. RESPONSIBILITY NOTICE

The authors are the only responsible for the printed material included in this paper.